Journal of Alloys and Compounds 495 (2010) 217–223

Contents lists available at ScienceDirect

Journal of Alloys and Compounds

journal homepage: www.elsevier.com/locate/jallcom

# Study on the influence of annealing temperature and ferrite content on the structural and magnetic properties of $x(NiFe_2O_4)/(100-x)SiO_2$ nanocomposites

Mehrnaz Gharagozlou*

*Department of Nanotechnology and Nanomaterials, Institute for Color Science and Technology, P.O. Box 16765-654, Tehran, Iran*

ARTICLE INFO

*Article history:*
Received 7 December 2009
Received in revised form 20 January 2010
Accepted 22 January 2010
Available online 4 February 2010

*Keywords:*
Nanocomposite
Ni-ferrite
Magnetic properties
Silica matrix
Sol–gel

ABSTRACT

Magnetic nanocomposites of nickel ferrite nanoparticles uniformly dispersed in the silica matrix have been synthesized successfully by a sol–gel process using tetraethylorthosilicate (TEOS) and metallic nitrates as precursors. In addition, the influence of the annealing temperatures, varying from 400 to 900 °C, and $NiFe_2O_4$ contents, $x(NiFe_2O_4)/(100-x)SiO_2$ ($10 \le x \le 60$ wt.%), on the structural and magnetic properties of the nanocomposite samples have been investigated. The studies carried out using XRD, FT-IR, TEM, STA (TG–DTG–DTA) and VSM techniques. The results indicated that the structural and magnetic properties of the samples showed great dependence on the variation of the particle size caused by the annealing temperature and $NiFe_2O_4$ content. The crystallization, saturation magnetization $M_s$ and remenant magnetization $M_r$ increased as the annealing temperature and $NiFe_2O_4$ content increase. But the variation of coercivity $H_c$ was not in accordance with that of $M_s$ and $M_r$, indicating that $H_c$ is not determined only by the size of $NiFe_2O_4$ nanoparticles. TEM images showed spherical nanoparticles homogeneously dispersed in the silica network and were uniform in both morphology and particle size distribution with sizes of 10–15 nm. The results showed that the well-established silica network provided nucleation locations for $NiFe_2O_4$ nanoparticles to confinement the coarsening and aggregation of nanoparticles. The synthesized nanocomposites with adjustable particle sizes and controllable magnetic properties make the applicability of nickel ferrite even more versatile.



## 1. Introduction

Magnetic nanocomposites consisting of nanometric spinel ferrites embedded in an insulating matrix such as silica have attracted much attention in recent years due to their new magnetic properties [1] and their applicability in a variety of areas such as magnetic recording media, high-density information storage, ferrofluid technology, bioprocessing, magnetic drug delivery, catalysts, magnetic resonance imaging enhancement, gas sensors and magneto-optical devices [2–9].

Among spinel ferrites, nickel ferrite is one of the most versatile and technologically important ferrite materials because of its magnetic properties, high electrochemical stability, catalytic behavior, abundance in nature, low conductivity and thus lower eddy current losses [10]. In addition, $NiFe_2O_4$ is the most suitable material for device applications in the upper microwave and lower millimeter wave ranges. Apart from its technological importance in the electronic and magnetic industries, $NiFe_2O_4$ has been used as a highly reproducible gas [9,11] and humidity [12] sensor material.

Various synthetic routes have been reported in the literature for the preparation of nanoscale ferrites such as ceramic method [13], sol–gel [14], co-precipitation [15], solvent evaporation [16], hydrothermal [17], combustion [18], microemulsion [19] and citrate methods [20]. In the previous report, spinel cobalt ferrite nanoparticles have been synthesized by the polymeric precursor method [21]. While the nanoparticles obtained usually have a strong tendency to aggregate; this makes it very difficult to exploit their unique physical properties [22]. The preparation of magnetic nanocomposites through the dispersion of ferrite nanoparticles in a suitable matrix represents a route to obtain very fine nanoparticles by reducing particle agglomeration [23] leading to a narrow distribution of the dimensions. Also this technique allows one to stabilize the particles and study their formation reactions.

The interest in the preparation of magnetic nanocomposites has increased in the last years due to the properties presented by these materials, which are dependent on particle sizes, component ratio and distribution in the matrix. Magnetic nanocomposites showed considerable differences in the magnetic properties when compared with their equivalent pure and bulk materials. Different nanoparticles such as Fe [24], Ni [25], $Fe_2O_3$ [26], and NiZn-ferrite [27] dispersed in the silica matrix with applications in areas such as catalysis, sensors and electronic devices have been studied. Magnetic nanocomposites of nickel ferrite nanoparticles dispersed in

* Tel.: +98 21 22944184; fax: +98 21 22947537.
*E-mail address:* gharagozlou@icrc.ac.ir.

0925-8388/$ – see front matter © 2010 Elsevier B.V. All rights reserved.
doi:10.1016/j.jallcom.2010.01.128

the silica matrix have been studied [28–35] revealing behavior different from that of bulk systems and as a model for the study of small particles.

Among various synthetic routes, the sol–gel process offers some advantages in making inorganic composite materials containing highly dispersed magnetic particles. The process facilitates a good and homogeneous dispersion of the particles into the inorganic matrix. The porous nature of the sol–gel derived amorphous silica matrix is an excellent host for supporting different types of guest nanoparticles which provides nucleation sites for magnetic nanoparticles and minimizes the aggregation imposing an upper limit to the size of the particles. This method makes possible the introduction of various concentrations of different components in a matrix with molecular homogeneity, which can be vitreous or crystalline, either porous or densified.

In this paper, the influence of annealing temperature and $NiFe_2O_4$ content on the structural and magnetic properties of $x(NiFe_2O_4)/(100-x)SiO_2$ ($x$ = 10, 20, 30, 40, 50, 60 wt.%) nanocomposites prepared by sol–gel method has been reported aiming at tuning the magnetic properties of $NiFe_2O_4$ nanoparticles dispersed in a silica matrix and greatly expanding the range of applications by adjusting the annealing temperature and $NiFe_2O_4$ content. Also, the alcogel precursors with different weight percents of components have been investigated. Therefore, special attention is given to the correlation between the structural and magnetic properties of $NiFe_2O_4$ nanoparticles embedded in a silica matrix, for different annealing temperatures and component ratios.

## 2. Experimental

All the chemicals were of analytical grade and used without any further purification. Nanocomposites of nickel ferrite dispersed in a silica matrix were prepared by sol–gel process using tetraethylorthosilicate (TEOS) as a precursor of silica and metallic nitrates as precursors of the ferrite. The TEOS:EtOH:$H_2O$ and Fe:Ni molar ratios were controlled at 1:4:8 and 2:1, respectively. The weight ratios of the nanocomposites were $x(NiFe_2O_4)/(100-x)SiO_2$ ($x$ = 10, 20, 30, 40, 50, 60 wt.%). The sols were prepared by dissolving $Fe(NO_3)_3{\cdot}9H_2O$ and $Ni(NO_3)_2{\cdot}6H_2O$ in deionized water, followed by the addition of the alcoholic solution of TEOS. After vigorous stirring for 1 h, the sols were allowed to gel at room temperature for 4 days in partially closed glass vessels. The obtained alcogels G1–G6 matching to $x$ = 10–60 wt.%, respectively were put into an oven for further drying at 110 °C for 24 h to obtain xerogels. The xerogels were annealed at different temperatures varying from 400 to 900 °C for 2 h with a heating rate of 10 °C/min in ambient atmosphere.

X-ray diffraction (XRD) patterns were collected using a Philips PNA-analytical diffractometer with Cu Kα radiation. FT-IR spectra (500–4000 $cm^{-1}$) were recorded on a PerkinElmer Spectrum One spectrophotometer with KBr pellets. Thermal analyses (TG–DTG–DTA) including the thermogravimetery (TG), derivative thermogravimetery (DTG) and differential thermal analysis (DTA) were carried out using a PerkinElmer simultaneous thermal analyzer (STA Pyris Diamond Model) with the heating rate of 5 °C/min in flowing air. TEM images were recorded on a Philips CM 200 FEG transmission electron microscope. Selected area electron diffraction (SAED) patterns were obtained on the TEM to ascertain the crystallinity. Magnetic measurements were carried out at room temperature using a vibrating sample magnetometer (VSM).

## 3. Results and discussion

### 3.1. X-ray diffraction (XRD) analysis

The XRD patterns of the 30 wt.% $NiFe_2O_4/SiO_2$ samples annealed at different temperatures varying from 400 to 900 °C were shown in Fig. 1 to investigate the influence of the annealing temperature on the structure. The weak diffraction peaks assigned to $NiFe_2O_4$ appeared at 400 °C suggesting that the particles of $NiFe_2O_4$ had been nucleated in the silica matrix.

Our results showed that with increasing the annealing temperature, the intensity of peaks increases and the diffraction peaks become sharper and narrower. This indicates the enhancement of the crystallinity which originated from the increment of the crystalline volume ratio due to the size enlargement of the nuclei

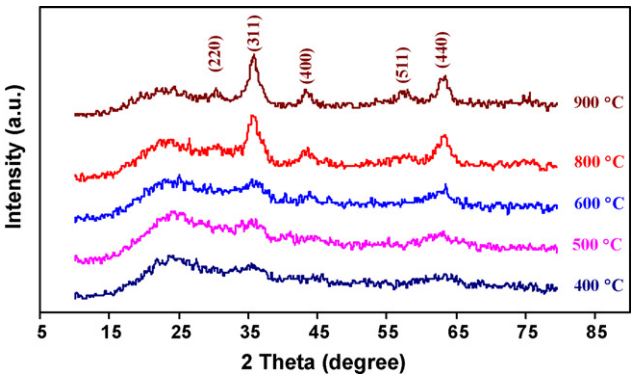


**Fig. 1.** XRD patterns of the 30 wt.% $NiFe_2O_4/SiO_2$ samples annealed at different temperatures varying from 400 to 900 °C.

[36]. The full-width at half maximum (FWHM) of the diffraction peaks decreases with increasing annealing temperature discloses that the average crystallite size is becoming bigger correspondingly. The very broad peak at $2\theta$ of around 23° in XRD patterns of all samples was attributed to the characteristic diffraction peak of the amorphous $SiO_2$ matrix. All of the diffraction peaks confirmed the formation of the pure single-phase nickel ferrite with the face-centered cubic spinel phase and $Fd3m$ (2 2 7) space group. No diffraction peaks of impurities were observed in the patterns. It showed that Ni-ferrites synthesized successfully under current mild experimental conditions.

To study the influence of the $NiFe_2O_4$ content on the structure, the XRD analyses were done on the $x(NiFe_2O_4)/(100-x)SiO_2$ ($x$ = 10, 20, 30, 40, 50, 60 wt.%) nanocomposites annealed at 800 °C as shown in Fig. 2. As the $NiFe_2O_4$ content increases from 10 to 60 wt.%, the characteristic diffraction peaks of $NiFe_2O_4$ gradually grow and become stronger in intensity but narrower in FWHM, which indicates that the crystallite size of $NiFe_2O_4$ increases with increasing the $NiFe_2O_4$ content. When the $NiFe_2O_4$ content is up to 40 wt.%, the evidence of the amorphous silica almost disappears. The position of all peaks coincided with the characteristics peaks of the standard $NiFe_2O_4$ phase.

The increase of the annealing temperature and the Ni-ferrite content results in sharper peaks with the increased intensity and higher crystallization without changes in the obtained phases. The influence of the annealing temperature and Ni-ferrite content on the crystallite sizes of the nanocomposite samples were shown in Tables 1 and 2, respectively.

The crystallite size of all samples prepared at different annealing temperatures and Ni-ferrite contents estimated from XRD peak

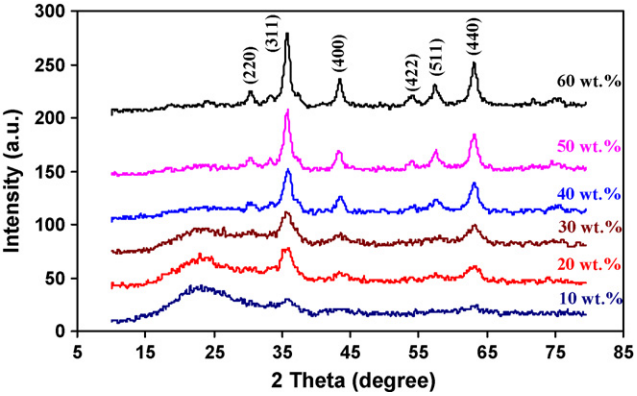


**Fig. 2.** XRD patterns of the $x(NiFe_2O_4)/(100-x)SiO_2$ ($x$ = 10, 20, 30, 40, 50, 60 wt.%) nanocomposites annealed at 800 °C.

**Table 1**
Magnetic properties of the 30 wt.% $NiFe_2O_4/SiO_2$ samples annealed at different temperatures varying from 400 to 900 °C.

| Temperature (°C) | Crystallite size (nm) | $M_s$ (emu/g) | $M_r$ (emu/g) | Coercivity, $H_c$ (Oe) |
|---|---|---|---|---|
| 400 | – | 0.14 | 0.001 | 23 |
| 500 | – | 0.18 | 0.003 | 28 |
| 600 | – | 0.55 | 0.012 | 45 |
| 800 | 7.9 | 2.87 | 0.017 | 19 |
| 900 | 10.8 | 4.65 | 0.042 | 8 |

**Table 2**
Magnetic properties of the $x(NiFe_2O_4)/(100-x)SiO_2$ ($x$ = 10, 20, 30, 40, 50, 60 wt.%) nanocomposites annealed at 800 °C.

| Ni-ferrite $x$ (wt.%) | Crystallite size (nm) | $M_s$ (emu/g) | $M_r$ (emu/g) | Coercivity, $H_c$ (Oe) |
|---|---|---|---|---|
| 10 | – | 1.37 | 0.010 | 19 |
| 20 | 7.3 | 2.85 | 0.011 | 6 |
| 30 | 7.9 | 2.87 | 0.016 | 20 |
| 40 | 9.3 | 7.57 | 0.149 | 8 |
| 50 | 10.8 | 7.62 | 0.560 | 21 |
| 60 | 13.2 | 9.15 | 0.302 | 12 |

broadening using Scherrer's formula [37]

$$t = \frac{0.9\lambda}{\beta \cos\theta} \quad (1)$$

where $t$ is the crystallite size, $\lambda$ the wavelength of X-ray radiation (Cu Kα), $\theta$ the Bragg angle and $\beta$ is the full-width at half maximum (FWHM) of the most intense diffraction peak (3 1 1). The crystallite size slightly increases only at higher annealing temperatures and Ni-ferrite contents, indicating that the silica network plays an important role in restricting the growth and aggregation of Ni-ferrite nanoparticles.

### 3.2. FT-IR analysis

Fig. 3 shows the FT-IR spectra of the alcogel G3 ($x$ = 30 wt.%) and 30 wt.% $NiFe_2O_4/SiO_2$ samples annealed at different temperatures varying from 400 to 900 °C.

Two broad bands at 3415 and 1633 $cm^{-1}$ in the IR spectrum of the alcogel G3 ascribed to the stretching mode and H–O–H bending vibration of the free or absorbed water. As shown in Fig. 3a, the band at 1384 $cm^{-1}$ is associated with the antisymmetric $NO_3^-$ stretching vibration arising from the residual nitrate groups in the alcogel. The silica network is characterized by the strong absorptions at 1079, 825 and 470 $cm^{-1}$ corresponding to the Si–O–Si antisymmetric stretching and bending modes [38].

In the IR spectra of the samples annealed at different temperatures varying from 400 to 900 °C, the intensities of the broad bands associated with the absorbed water are drastically weakened. Also, the disappearance of the absorption at 1384 $cm^{-1}$ could be ascribed to the complete decomposition of the nitrate species after annealing, as confirmed by the thermal analysis. The band at 580 $cm^{-1}$ assigned to the Si–O–Fe vibration increases in intensity with increasing the annealing temperature, which can be ascribed to the enhanced interactions between $NiFe_2O_4$ particles and the silica matrix [39]. The absence of the band at 580 $cm^{-1}$ showed the breakage of the Si–O–Fe interaction in samples annealed at 400 and 500 °C. The characteristic absorptions for the silica network slightly increased in intensity with increasing annealing temperature.

FT-IR spectra of the alcogels G1–G6 matching to $x$ = 10, 20, 40, 50, 60 wt.% were shown in Fig. 4. In the IR spectra the stretching mode and H–O–H bending vibration of the free or absorbed water appeared at about 3420 and 1635 $cm^{-1}$, respectively. All the alcogels showed the characteristic vibration of silica and nitrate precursors. The characteristic bands of the silica network decrease in intensity with increasing the Ni-ferrite content.

The FT-IR spectra of the $x(NiFe_2O_4)/(100-x)SiO_2$ ($x$ = 10, 20, 30, 40, 50, 60 wt.%) nanocomposites annealed at 800 °C were shown in Fig. 5. With increasing the Ni-ferrite content the intensity of ≡Si–O–Si≡ absorption band of the $SiO_4$ tetrahedron of the silica network at 1080 $cm^{-1}$ slightly decreases. The intensity of the

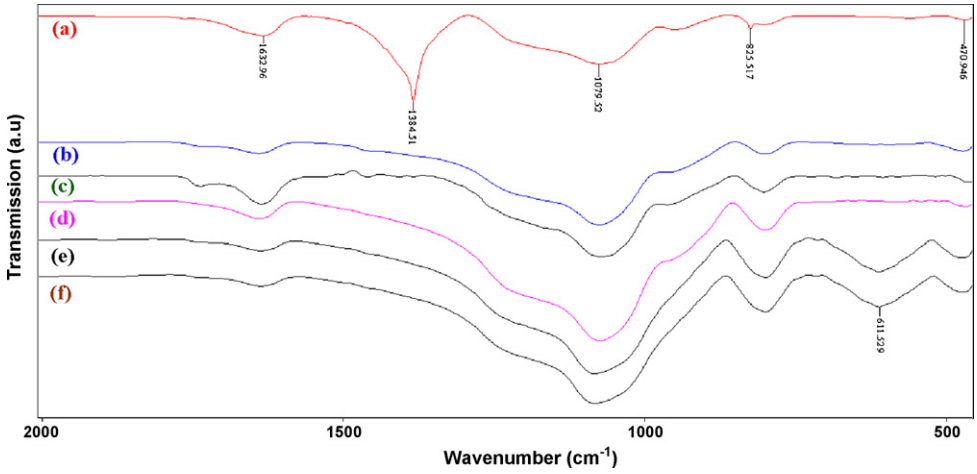


**Fig. 3.** FT-IR spectra of (a) alcogel G3 ($x$ = 30 wt.%) and 30 wt.% $NiFe_2O_4/SiO_2$ samples annealed at (b) 400 °C, (c) 500 °C, (d) 600 °C, (e) 800 °C, and (f) 900 °C.

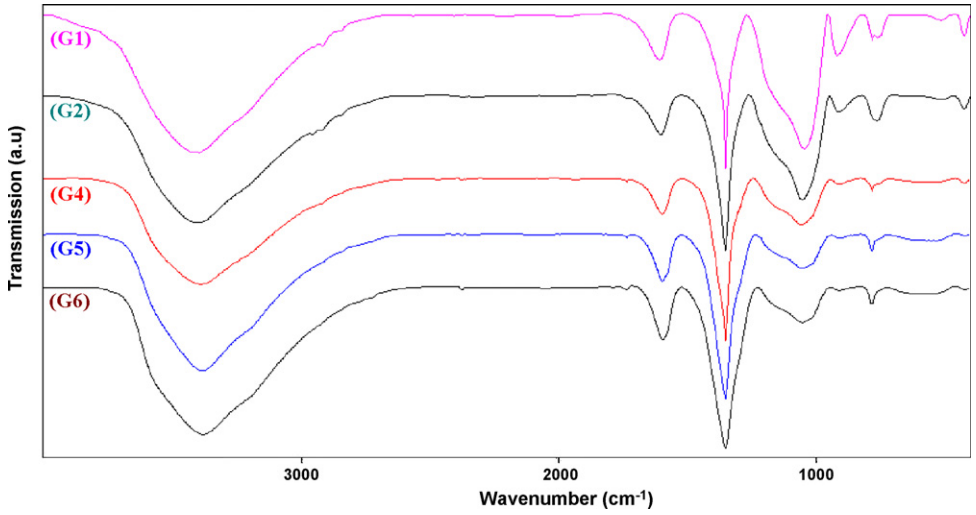


**Fig. 4.** FT-IR spectra of alcogels matching to $x = 10, 20, 40, 50, 60$ wt.%.

band assigned to Si–O–Fe vibrations increases with decreasing the $NiFe_2O_4$ content, which can be attributed to the enhanced interactions between $NiFe_2O_4$ particles and the silica matrix.

### 3.3. Thermal analysis

The simultaneous thermal analyses (TG–DTG–DTA) of the alcogel G3 matching to $x = 30$ wt.% were shown in Fig. 6. The thermogravimetery (TG) and derivative thermogravimetery (DTG) curves show two stages of the weight loss. The total weight loss is 70% up to 400 °C, typical of the synthesis processes using sol–gel routes. First stage of the weight loss at about 50–120 °C was attributed to the loss of water and some gases adsorbed on the surface, which corresponds to an endothermic peak in the differential thermal analysis (DTA) curve. The second one at about 150–350 °C was ascribed to the burning of residual $CH_3$–$CH_2$–O– groups accompanied by an exothermic peak in the DTA curve. We can observe a broad endothermic event between 600 and 1300 °C associated with the densification of the nanocomposites. Above 400 °C the weight loss is almost negligible showing that the majority of the mass loss occurs under 400 °C which allows for optimization of the heat treatment program. These results were in agreement with the FT-IR spectroscopy and XRD ones.

### 3.4. Transmission electron microscopy (TEM) analysis

The TEM images and selected area electron diffraction (SAED) patterns of the $x(NiFe_2O_4)/(100-x)SiO_2$ ($x = 30$ and 50 wt.%) nanocomposites annealed at 800 °C were shown in Fig. 7. TEM observations indicate that the uniformly dispersed, well-crystallized and almost spherical Ni-ferrite nanoparticles were homogeneously embedded in the silica network. The average particle sizes of the $x(NiFe_2O_4)/(100-x)SiO_2$ nanocomposites with $NiFe_2O_4$ content of 30 wt.% and 50 wt.% were about 10 nm and 14 nm, respectively, in accordance with the results obtained from XRD analyses according to the Scherrer's formula. The diffraction dots and diffuse rings of different lattice planes in the SAED patterns (Fig. 7c and d) were in good agreement with the present spinel system.

### 3.5. Magnetic measurements

To investigate the influence of the annealing temperature and Ni-ferrite content on the magnetic properties of the nanocomposite samples, hysteresis loops of the 30 wt.% $NiFe_2O_4/SiO_2$ samples annealed at different temperatures varying from 400 to 900 °C and $x(NiFe_2O_4)/(100-x)SiO_2$ ($x = 10, 20, 30, 40, 50, 60$ wt.%) nanocom-

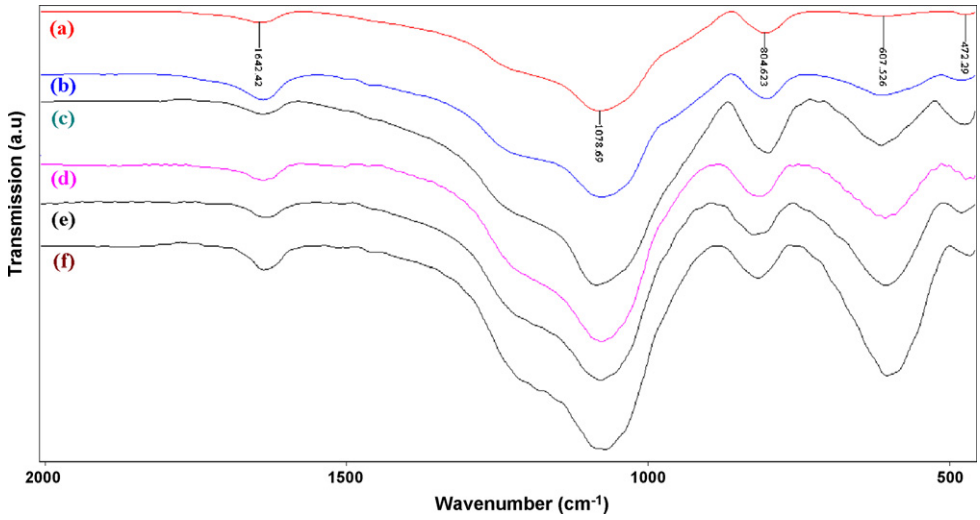


**Fig. 5.** FT-IR spectra of $x(NiFe_2O_4)/(100-x)SiO_2$ (a) $x = 10$ wt.%, (b) $x = 20$ wt.%, (c) $x = 30$ wt.%, (d) $x = 40$ wt.%, (e) $x = 50$ wt.% and (f) $x = 60$ wt.% annealed at 800 °C.

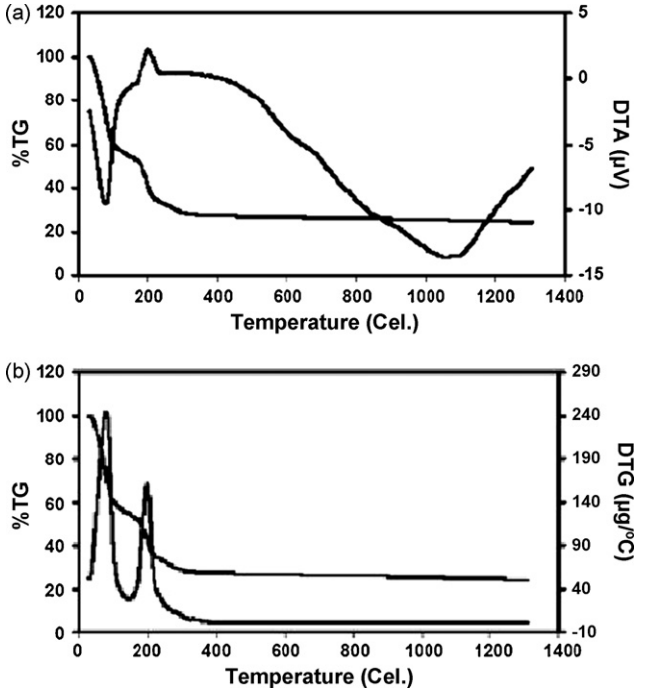


**Fig. 6.** Thermal analyses of the alcogel G3 ($x$ = 30 wt.%): (a) TG–DTA and (b) TG–DTG.

posites annealed at 800 °C were analyzed by VSM, as shown in Figs. 8 and 9, respectively. Also, the corresponding magnetic parameters were listed in Tables 1 and 2.

Our results showed that the magnetic remnant and coercivity values were negligible and also the curves of all samples did not reach saturation which indicates that the nanoparticles are mostly in superparamagnetic state. These results are in good agreement with previous data for nickel ferrite nanoparticles dispersed in the silica matrix [28–33]. Manova et al. [28], Liu et al. [30] and Mohallem and Seara [40] reported the superparamagnetic nanoparticles with the $M_S$ values less than 10 emu/g and negligible magnetic remnant and coercivity values for nanoparticles with size less than 15 nm. Kinemuchi et al. [41] found the value

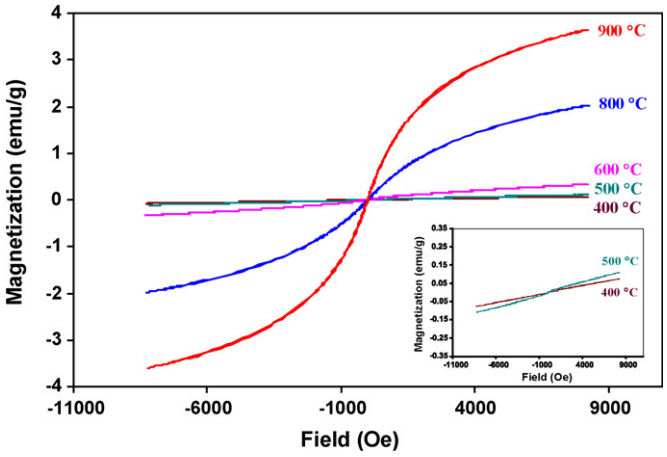


**Fig. 8.** Hysteresis loops of 30 wt.% $NiFe_2O_4/SiO_2$ samples annealed at different temperatures varying from 400 to 900 °C. The inset shows the higher magnification of 400 and 500 °C.

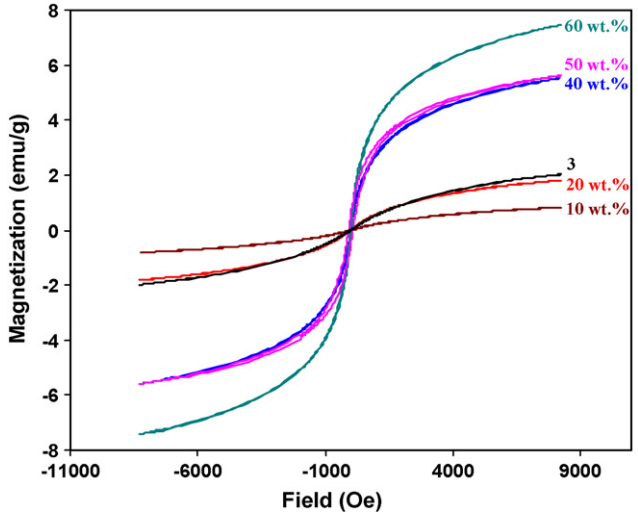


**Fig. 9.** Hysteresis loops of $x(NiFe_2O_4)/(100-x)SiO_2$ ($x$ = 10, 20, 30, 40, 50, 60 wt.%) nanocomposites annealed at 800 °C.

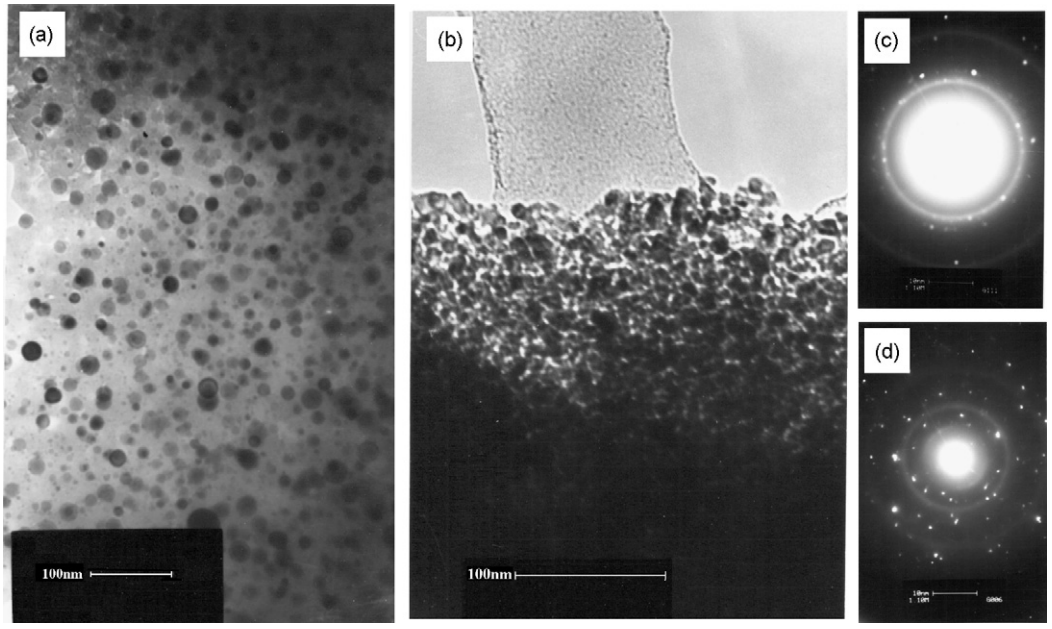


**Fig. 7.** TEM micrographs: (a) $x$ = 30 wt.%, (b) $x$ = 50 wt.%; SAED patterns: (c) $x$ = 30 wt.%, (d) $x$ = 50 wt.% of $x(NiFe_2O_4)/(100-x)SiO_2$ nanocomposites annealed at 800 °C.

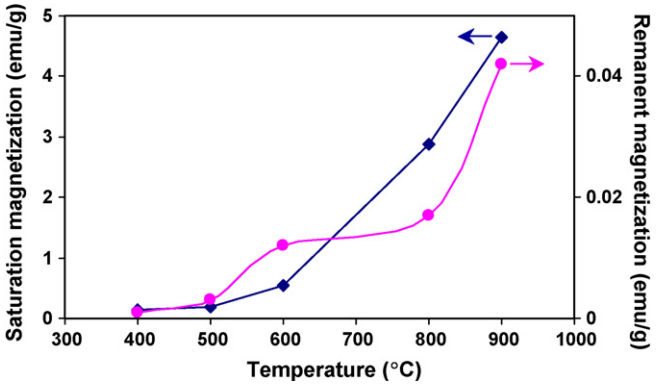


**Fig. 10.** Variation of saturation magnetization ($M_s$) and remanent magnetization ($M_r$) of 30 wt.% $NiFe_2O_4/SiO_2$ samples annealed at different temperatures varying from 400 to 900 °C as a function of the annealing temperature.

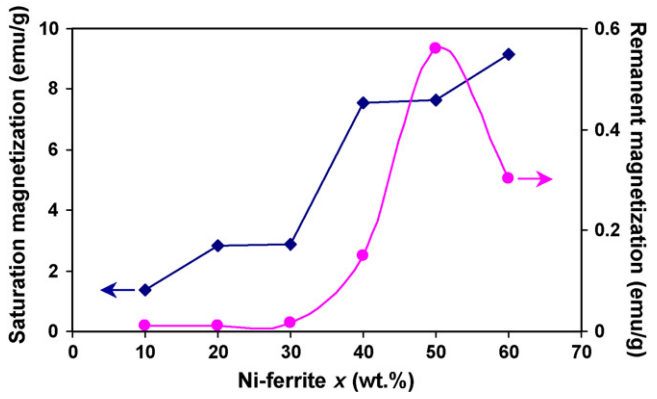


**Fig. 11.** Variation of saturation magnetization ($M_s$) and remanent magnetization ($M_r$) of the $x(NiFe_2O_4)/(100-x)SiO_2$ ($x$ = 10, 20, 30, 40, 50, 60 wt.%) nanocomposites annealed at 800 °C as a function of the Ni-ferrite $x$ (wt.%).

of 33 emu/g for nanoparticles with size of 45 nm. While Huang and Chen reported nanocomposites prepared through solutions containing $HNO_3$ [34] which showed ferromagnetic behavior with significant magnetic remnant values and coercivity can get value as high as 313 Oe.

It seems that 30 wt.% $NiFe_2O_4/SiO_2$ samples annealed at 800 and 900 °C have typical superparamagnetic behavior, while samples annealed at lower temperatures, 400–600 °C, are paramagnetic and showed a drastic change in the shape of hysteresis loop (Fig. 8). In addition, typical superparamagnetic behavior observed for $x(NiFe_2O_4)/(100-x)SiO_2$ ($x$ = 20, 30, 40, 50, 60 wt.%) samples, whereas the 10 wt.% $NiFe_2O_4/SiO_2$ sample showed the paramagnetic behavior. Below the critical size, $NiFe_2O_4$ nanocrystals had a superparamagnetic single domain structure, while the nanocrystals with particle sizes larger than the critical size exhibited bulk like behavior.

The variation of the saturation magnetization $M_s$ and remanent magnetization $M_r$ as a function of temperature and $NiFe_2O_4$ content were shown in Figs. 10 and 11, respectively. To calculate the saturation magnetization ($M_s$) the magnetization values ($M$) were plotted vs. $1/H$. The $M_s$ was calculated from the extrapolation of the magnetic curve at the magnitude of $M$ when $1/H \approx 0$ (Tables 1 and 2). It can be observed that the $M_s$ and $M_r$ values for 30 wt.% $NiFe_2O_4/SiO_2$ samples annealed at different temperatures were increased by increasing the temperature (Fig. 10), whereas the coercivity increases with the annealing temperature then decreases, which is in agreement with the literature [39]. This type of behavior is entirely consistent with a model of particle growth in the system in such a way that the differences in the magnetic parameters are associated with changes in the particle size [42]. Fig. 11 showed that $M_s$ values for $x(NiFe_2O_4)/(100-x)SiO_2$ ($x$ = 10, 20, 30, 40, 50, 60 wt.%) samples increased by increasing the $NiFe_2O_4$ content, while the coercivity showed no regular orderliness.

The changes in the magnetic properties of the samples can be recognized by the modification of the crystallite sizes dependent on the annealing temperature and $NiFe_2O_4$ content [43]. Our results show that the saturation magnetization values of the samples increase with increasing the particle sizes due to the spin non-colinearity at the surface of the crystals, while the coercivity field values have no analogous orderliness. These properties originate from the large surface area, reduced size and modification in interparticle interactions. Due to the proportionality of the magnetic particle energy in the external field to the particle sizes via the number of molecules in a single magnetic domain, the increase of the $M_s$ values with the increase of particle sizes can be attributed to the surface effects which are the result of the finite-size scaling [44] of nanocrystallites.

The lower $M_s$ values related to the particles with the smaller size could be attributed to the surface distortion due to the interaction of transition metal ions in the spinel lattice with the oxygen atoms, which can reduce the net magnetic moment in the particle [45]. This effect is particularly prominent for the ultrafine particles due to their large surface to volume ratio. In addition, the magnetocrystalline anisotropy of the particles is dependent on the degree of the crystallinity of the nanoparticles. Large proportion of crystal defects and dislocations can occur within the lattice of most samples annealed at lower temperatures which causes a significant reduction of the magnetic moment within the particles as a result of the magnetocrystalline anisotropy distortion. In all samples the saturation magnetization values were in good agreement with previous reports [28,30–32,40] and were less than the value reported for the bulk $NiFe_2O_4$ (55 emu/g) [46]. Finite-size effects have been reported as being responsible for the reduction of the saturation magnetization of nanoparticles [47].

## 4. Conclusions

In summary, the influence of the annealing temperature and Ni-ferrite content on the magnetic properties and crystallite size of the $x(NiFe_2O_4)/(100-x)SiO_2$ ($10 \le x \le 60$ wt.%) nanocomposites with tunable magnetic properties which successfully synthesized by sol–gel route were investigated with the aim of tuning the magnetic properties and greatly expanding the range of applications. The silica matrix network provides an ideal nucleation environment to uniformly disperse $NiFe_2O_4$ nanoparticles and thus to confine them to aggregate and coarsen. Particle sizes of the samples increased with the annealing temperature and Ni-ferrite content. Our results showed that the magnetic properties of the nanocomposite samples were strongly affected by the annealing temperature and Ni-ferrite content as a consequence of the gradual increase in the crystallinity and particle size. The saturation magnetization for all the samples was lower than that of the $NiFe_2O_4$ bulk phase owing to the particle sizes obtained. Therefore, uniformly dispersed, size-adjustable and magnetic controllable nickel ferrite nanoparticles were obtained by embedding $NiFe_2O_4$ particles in the amorphous silica network and controlling suitable annealing temperature and $NiFe_2O_4$ content. The magnetic properties of the synthesized nanocomposites indicate that these materials have good potential for important technological applications, e.g. in information storage, bioprocessing and magneto-optical devices.

## Acknowledgment

We are grateful to the Research Council of Institute for Color Science and Technology for their financial support.

## References

[1] C.L. Chien, Annu. Rev. Mater. Sci. 25 (1995) 129.
[2] I. Anton, I.D. Dabata, L. Vekas, J. Magn. Magn. Mater. 85 (1990) 219.
[3] L. Gunther, Phys. World 3 (1990) 28.
[4] R.D. McMickael, R.D. Shull, L.J. Swartzendruber, L.H. Bennett, R.E. Watson, J. Magn. Magn. Mater. 111 (1992) 29.
[5] J. Popplewell, L. Sakhnini, J. Magn. Magn. Mater. 149 (1995) 72.
[6] R.S. Molday, D. Mackenzie, J. Immunol. Methods 52 (1982) 353.
[7] H.H. Kung, M.C. Kung, Adv. Catal. 33 (1985) 159.
[8] C.W. Jung, P. Jacobs, J. Magn. Reson. Imaging 13 (1995) 661.
[9] C.V. Gopal Reddy, S.V. Manorama, V.J. Rao, J. Mater. Sci. Lett. 19 (2000) 775.
[10] B. Baruwati, K. Reddy, S. Manorama, R. Singh, O. Parkash, Appl. Phys. Lett. 85 (2004) 2833.
[11] C.V. Gopal Reddy, S.V. Manorama, V.J. Rao, Sens. Actuators B 55 (1990) 90.
[12] G. Dube, V. Darshane, J. Mol. Catal. 79 (1993) 285.
[13] D.W. Johnson, B.B. Ghate, F.Y. Wang, Advances in Ceramics, vol. 15, American Ceramic Society, Columbus, OH, 1985, p. 27.
[14] E. Veena Gopalan, P.A. Joy, I.A. Al-Omari, D. Sakthi Kumar, Y. Yoshida, M.R. Anantharaman, J. Alloys Compd. 485 (2009) 711.
[15] Y. Wang, G. Xu, L. Yang, Z. Ren, X. Wei, W. Weng, P. Du, G. Shen, G. Han, Ceram. Int. 35 (2009) 1285.
[16] P. Priyadharsini, A. Pradeep, G. Chandrasekaran, J. Magn. Magn. Mater. 321 (2009) 1898.
[17] J. Wang, P.F. Chong, S.C. Ng, L.M. Gan, Mater. Lett. 30 (1997) 217.
[18] P. Ravindranathan, K.C. Patil, Am. Ceram. Soc. Bull. 66 (1987) 688.
[19] V. Pillai, D.O. Shah, J. Magn. Magn. Mater. 163 (1996) 243.
[20] M. Lal, D.K. Sharma, M. Singh, Indian J. Pure Appl. Phys. 43 (2005) 291.
[21] M. Gharagozlou, J. Alloys Compd. 486 (2009) 660.
[22] K.H. Wu, C.H. Yu, Y.C. Chang, D.N. Horng, J. Solid State Chem. 177 (2004) 4119.
[23] Z.H. Zhou, J.M. Xue, H.S.O. Chan, J. Wang, Mater. Chem. Phys. 75 (2002) 181.
[24] W. Jian-Ping, L. He-Lie, J. Magn. Magn. Mater. 131 (1994) 54.
[25] O.C. Gonzalez, C. Estournes, M.R. Plouet, J.L. Guille, Mater. Sci. Eng. C 15 (2001) 179.
[26] F.D. Monte, M.P. Morales, D. Levy, A. Fernandez, M. Ocana, A. Roig, E. Molins, K.O. Grady, C.J. Serna, Langmuir 13 (1997) 3627.
[27] S.P. Castaneda, J.R. Martinez, S.A. Palomares Sanchez, F. Ruiz, J.A. Matutes Aquino, J. Sol–Gel Sci. Technol. 25 (2002) 37.
[28] E. Manova, T. Tsoncheva, D. Paneva, J.L. Rehspringer, K. Tenchev, I. Mitov, L. Petrov, Appl. Catal. A 317 (2007) 34.
[29] L. Guang-She, L. Li-Ping, R.L. Smith Jr., H. Inomata, J. Mol. Struct. 560 (2001) 87.
[30] X.M. Liu, S.Y. Fu, C.J. Huang, J. Magn. Magn. Mater. 281 (2004) 234.
[31] S. Mitra, K. Mandal, P.A. Kumar, J. Magn. Magn. Mater. 306 (2006) 254.
[32] H. Wang, W. Zhang, F. Zhang, Y. Cao, W. Su, J. Magn. Magn. Mater. 320 (2008) 1916.
[33] H. Wang, F. Zhang, W. Zhang, X. Wang, Z. Lu, Z. Qian, Y. Sui, D. Dong, W. Su, J. Cryst. Growth 293 (2006) 169.
[34] X. Huang, Z. Chen, J. Magn. Magn. Mater. 280 (2004) 37.
[35] X. Huang, Z. Chen, Mater. Res. Bull. 40 (2005) 105.
[36] Y.P. Sui, X.F. Huang, Z.Y. Ma, W. Li, F. Qiao, K. Chen, K.J. Chen, J. Phys.: Condens. Matter 15 (2003) 5793.
[37] B.D. Cullity, Elements of X-ray Diffraction, Addison-Wesley Publishing Company, Reading, MA, 1956, p. 259.
[38] H. Izutsu, P.K. Nair, K. Maeda, Y. Kiyozumi, F. Mizukami, Mater. Res. Bull. 32 (1997) 1303.
[39] C. Caizer, M. Stefanescu, J. Phys. D: Appl. Phys. 35 (2002) 3035.
[40] N.D.S. Mohallem, L.M. Seara, Appl. Surf. Sci. 214 (2003) 143.
[41] Y. Kinemuchi, K. Ishizaka, H. Suematsu, W. Jiang, K. Yatsui, Thin Solid Films 407 (2002) 109.
[42] A.E. Berkowitz, W.J. Schuele, P.J. Flanders, J. Appl. Phys. 39 (1968) 1261.
[43] K.V.P.M. Shafi, A. Gedanken, R. Prozorov, J. Balogh, Chem. Mater. 10 (1998) 3445.
[44] R.H. Kodama, A.E. Berkowitz, E.J. Mcniff, S. Foner, Phys. Rev. Lett. 77 (1996) 394.
[45] M. Rajendran, R.C. Pullar, A.K. Bhattacharya, D. Das, S.N. Chintalapudi, C.K. Majumdar, J. Magn. Magn. Mater. 232 (2001) 71.
[46] J. Smit, H.P. Wijin, Ferrites, Philips Technical Library, Eindhoven, The Netherlands, 1959, p. 157.
[47] J.M.D. Coey, Phys. Rev. Lett. 27 (1971) 1140.